Adaptive Narrowband Damping for Improving Harmonic Stability of Modular Multilevel Converter

Preprint

Pengxiang Huang and Shahil Shah

National Renewable Energy Laboratory

Presented at the 23rd Wind & Solar Integration Workshop
Helsinki, Finland
October 8–11, 2024

NREL is a national laboratory of the U.S. Department of Energy
Office of Energy Efficiency & Renewable Energy
Operated by the Alliance for Sustainable Energy, LLC

This report is available at no cost from the National Renewable Energy Laboratory (NREL) at www.nrel.gov/publications.

Contract No. DE-AC36-08GO28308

Conference Paper
NREL/CP-5D00-91149
October 2024

Adaptive Narrowband Damping for Improving Harmonic Stability of Modular Multilevel Converter

Preprint

Pengxiang Huang and Shahil Shah

National Renewable Energy Laboratory

Suggested Citation
Huang, Pengxiang, and Shahil Shah. 2024. *Adaptive Narrowband Damping for Improving Harmonic Stability of Modular Multilevel Converter: Preprint*. Golden, CO: National Renewable Energy Laboratory. NREL/CP-5D00-91149.
https://www.nrel.gov/docs/fy25osti/91149.pdf.

NREL is a national laboratory of the U.S. Department of Energy
Office of Energy Efficiency & Renewable Energy
Operated by the Alliance for Sustainable Energy, LLC

This report is available at no cost from the National Renewable Energy Laboratory (NREL) at www.nrel.gov/publications.

Contract No. DE-AC36-08GO28308

Conference Paper
NREL/CP-5D00-91149
October 2024

National Renewable Energy Laboratory
15013 Denver West Parkway
Golden, CO 80401
303-275-3000 • www.nrel.gov

NOTICE

This work was authored by the National Renewable Energy Laboratory, operated by Alliance for Sustainable Energy, LLC, for the U.S. Department of Energy (DOE) under Contract No. DE-AC36-08GO28308. Funding provided by U.S. Department of Energy Office of Energy Efficiency and Renewable Energy Wind Energy Technologies Office. The views expressed herein do not necessarily represent the views of the DOE or the U.S. Government.

Cover Photos by Dennis Schroeder: (clockwise, left to right) NREL 51934, NREL 45897, NREL 42160, NREL 45891, NREL 48097, NREL 46526.

ADAPTIVE NARROWBAND DAMPING FOR IMPROVING HARMONIC STABILITY OF MODULAR MULTILEVEL CONVERTER

Pengxiang Huang, Shahil Shah*

National Renewable Energy Laboratory, Golden, CO United States
**shahil.shah@nrel.gov*

Keywords: HARMONIC STABILITY, ACTIVE DAMPING, ADAPTIVE CONTROL, ONLINE DETECTION

Abstract

Harmonic instability events between modular multilevel converter (MMC) and ac systems have been widely reported in recent years. To damp harmonic resonance, this paper proposes an adaptive narrowband damping control that automatically programs, adds, and adjusts the damping around the oscillation frequency when an oscillation is detected. First, the paper presents a low-pass filter design for MMC control loops that pushes all negative damping of the MMC impedance down to the medium-frequency range ($< \sim 1000$ Hz). Then, an adaptive damping control that uses online oscillation detection is proposed, which can automatically configure the narrowband damper to provide positive damping to the MMC around the detected oscillation frequency. In contrast to existing narrowband damping methods, the proposed adaptive narrowband damper dynamically adjusts the damping gain and the width of the damping range based on continuous monitoring of system resonance conditions (e.g., adjust damping gain to zero when the system resonance disappears). Electromagnetic transient simulation results validate the efficacy of the proposed method in two typical MMC-based power systems.

1 Introduction

In recent years, harmonic instability events (beyond the second harmonic frequency) have been widely reported in several modular multilevel converter (MMC)-based high-voltage dc (HVDC) systems, including both land-based [1] and offshore sides [2]. These harmonic instability events are rooted in the fact that the system resonance frequency falls within the negative damping region of the impedance response of MMC induced by time delays [3]. To mitigate such harmonic oscillations, several methods have been extensively studied in the literature. Among all of these methods, active methods are particularly attractive since they offer a controllable frequency range and degree of damping added to MMC impedance, while avoiding costs of power loss and additional installation space associated with passive methods. (especially for offshore applications).

Active methods generally fall into two categories, wideband methods [1, 4] and narrowband methods [4, 5]. Depending on whether the damping function is connected in parallel or in series with the controller, wideband methods can be further classified into wideband filtering and wideband damping. In the former, low-pass filters with a few 100s of bandwidth or even lower are usually inserted into the current and voltage control loops of the MMC, effectively eliminating negative damping of the MMC impedance within the stopband of low-pass filters. In current MMC projects, this is widely used to prevent harmonic oscillations; however, the delay-related phase lag subjected by the filter, when combined with the inherent phase shift of the filter in its passband and transition band, can significantly increase the negative damping of MMC impedance and worsen any resonance in the frequency range of passband of low-pass filter. Another impact is that an extremely low bandwidth of low-pass filter may deteriorate the controller stability and desired dynamics. In addition, wideband damping can be introduced by feeding the ac current and voltage measurement to the damping control function and directly adding the output to the modulation signals. Several damping functions have been proposed in the literature to minimize the negative damping region of power converters [4, 5], while only the method in [4] that incorporates a passivity-based controller can make the MMC impedance completely passive from the second harmonic frequency and the damping effect is not affected by the amount of delay; however, because the passivity-based controller uses both current and voltage feedforward and its broadband characteristic, it inevitably deteriorates the ride-through capability of the MMC controllers.

Similar to wideband methods, narrowband methods can also be divided into narrowband filtering using notch filters [6] and narrowband damping [7] utilizing band-pass filters. Narrowband filtering is generally not recommended because the time delay effect coupled with notch filter's inherent phase shift can cause more negative damping around its stopband. On the other hand, narrowband damping uses a band-pass filter along with a damping

function [7], which can add positive damping to the MMC impedance within a selected narrow frequency range and compensate for the time delay effect via a phase-leading unit. This method does not affect the characteristic of the MMC outside the selected damping range, thus avoiding the problems associated with other methods mentioned above. However, because harmonic oscillations cannot be predicted offline and their frequency can change with varying system configurations, a narrowband damping function needs to be employed in conjunction with online oscillation detection, which is referred to as adaptive narrowband damping [7, 8]; however, several issues related to adaptive narrowband damping control remain unresolved in the existing literature: 1) The existing design of the damper gain aims to ensure that the impedance of the MMC at the resonance frequency does not change before and after applying the damper. Although such a design avoids the resonance frequency shift caused by the damper, when the negative damping of the MMC impedance is large, it might significantly change the impedance magnitude of the MMC outside the damping range. As a consequence, it can develop a new resonance between the MMC and the ac system. 2) The existing literature does not provide a guideline for selecting the bandwidth of the narrow damper, nor does it discuss the impact that the improper selection of the bandwidth might have on the damping performance and system stability. 3) The main focus of the adaptivity of the existing adaptive narrowband damping control is on the capability to activate the damper in response to the detected resonance frequency; however, the methods for adjusting the damper's gain and bandwidth according to specific system resonance conditions, as well as the automatic deactivation of the damper when thes resonance conditions disappear, have not been explored.

An important feature of harmonic oscillations is that multiple harmonic oscillations can occur simultaneously, and their frequencies vary with changes in the system configuration, posing additional challenges for both existing wideband and narrowband methods. Considering the low-pass filter is effective at removing negative damping of MMC impedance above its cutoff frequencies, first, this paper discusses how low-pass filter can be designed to limit the negative damping of the MMC impedance within the medium-frequency range without affecting the controller dynamics. By doing so, the issue of multiple harmonic oscillations is converted to a single harmonic oscillation within the medium-frequency range. Then, this work proposes an adaptive narrowband damper that can, via the adaptive tuning unit, dynamically adjusts its damping gain and damping width according to the damping requirement of the system and the intensity of current or voltage oscillations. In addition, the narrowband damping function, if the resonance condition is no longer present, can also be automatically deactivated based on the proposed adaptive tuning method.

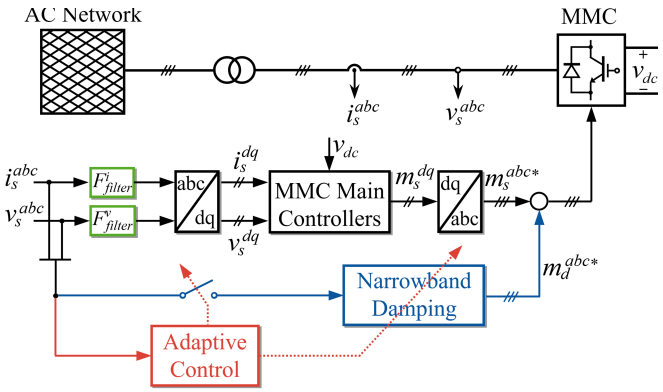

Fig. 1. Diagram of system under study

2 MMCs and System Description

2.1 System Description and Impedance Model of MMCs

Fig. 1 presents a simplified schematic of an MMC-based system, which also indicates how the proposed adaptive narrowband damping control should be introduced. Note that it includes an adaptive control unit that adaptively activates/deactivates and adjusts the narrowband damping control function (denoted as $H_d(s)$) based on continuous monitoring of the system's resonance conditions. The MMC in Fig.1 can be operated as either a grid-following MMC or a grid-forming MMC, depending on whether the MMC regulates its ac output current or voltage. The ac network in this context can be a passive grid (e.g., series-compensated grid, overhead lines) or an "active" system dominated by power converters (e.g., offshore wind plant). The electrical and control parameters for the MMC are tabulated in Tables 1 and 2.

Because this paper focuses on the harmonic stability, several key points should be emphasized when modeling MMC impedance:

- The transfer functions relating the ac-side perturbations at f_p to the ac-side responses at $f_p - 2f_1$ and

Table 1 Electrical Parameters for MMCs

Parameter	Symbol	Value	Unit
Rated active power	P_N	900	MW
Rated ac-side voltage	U_N	300	kV RMS ph-ph
Rated dc-side voltage	V_{dc}	±320	kV
Arm reactor impedance	$R_s + jL_s$	$0.1 + j0.05$	Ω
Submodules per arm	N_{sm}	200	N/A
Submodule capacitance	C_{sm}	4.66	mF
Time delay	e^{-sT_d}	450	μs

Table 2 Control Specifications for MMCs

Control Mode	K_p	K_i	K_d
dc voltage control	0.0065	0.2	NA
ac current control	22.2	27915.5	7.85
Circulating current control	22.2	13957.7	31.42
Active/reactive power control	1.5	300	N/A
Phase-locked loop	1.48×10^{-4}	0.0093	N/A
ac voltage control	0.5	54.4	N/A

Table 3 $G_i(s)$ and $G_v(s)$ in Different Control Modes

Control Modes	Forms of $G_i(s)$ and $G_v(s)$
V_{dc} & $Q=0$	$G_i(s)=F^i_{filter}(s)[H_i(s-j\omega_1)-jK_c]$ $G_v(s)=0$
P & Q	$G_i(s)=F^i_{filter}(s)H_i(s-j\omega_1)[1+1.5V_dH_p(s-j\omega_1)]$ $G_v(s)=0$
V_{dc} & Q	$G_i(s)=F^i_{filter}(s)H_i(s-j\omega_1)[1+0.75V_dH_p(s-j\omega_1)]$ $G_v(s)=-0.75(I_d+jI_q)F^i_{filter}(s)H_i(s-j\omega_1)H_p(s-j\omega_1)$
V_{ac} & f (single-loop)	$G_i(s)=0$ $G_v(s)=F^v_{filter}(s)H_v(s-j\omega_1)$
V_{ac} & f (dual-loop)	$G_i(s)=F^i_{filter}(s)[H_i(s-j\omega_1)-jK_c]$ $G_v(s)=F^v_{filter}(s)H_v(s-j\omega_1)H_i(s-j\omega_1)]$

to the dc-side responses at f_p-f_1 include multiple low-pass filtering stages, which are formed by the admittance of the arm inductor and the impedance of the submodule capacitors.

- The dynamics of the circulating current suppressing control and the energy balancing control are highly dependent on the dynamics of the sum of the submodule capacitor voltages, which are typically slow.
- Due to the second-order low-pass structure of a phase-locked loop's closed-loop transfer function, a phase-locked loop response to small-signal disturbances in the harmonic frequency range is relatively small.
- AC droop control affects the grid-forming MMC's dynamics around only the fundamental frequency [9].

Given these points, dc voltage control, circulating current suppressing control, energy balancing control, phase-locked loop, and droop control can be ignored when modeling MMC impedance within the harmonic frequency range; therefore, the simplified impedance models of MMC are given by:

$$Z_p(s)=\frac{sL+e^{-sT_d}G_i(s)}{1+e^{-sT_d}G_v(s)}=\frac{N_p(s)}{D_p(s)}=\frac{1}{Y_p(s)} \tag{1}$$

where sL is half of the MMC arm inductance; and $G_i(s)$ and $G_v(s)$ describe the current- and voltage-related control effects, which come in different forms based on the control modes adopted by the MMC, as shown in Table 3. In Table 3, $H_i(s-j\omega_1)$, $H_p(s-j\omega_1)$, $H_v(s-j\omega_1)$, and K_c represent the inner current controller, outer power controller, outer ac voltage controller, and current decoupling gain in the dq-reference frame, respectively. $F^i_{filter}(s)$ and $F^v_{filter}(s)$ are the low-pass filters used in the current and voltage measurements.

2.2 Damping Control and Its Effect on MMC

As shown in Fig. 1, the narrowband damping control uses ac voltage as its input and adds the output directly to the modulation signal. The effects of it can be modeled by replacing $G_v(s)$ in (1) by $G_v(s)+H_d(s)$, and the admittance of MMC with such narrowband damper is given as:

$$\begin{aligned}Y^d_p(s)&=\frac{1+e^{-sT_d}[G_v(s)+H_d(s)]}{sL+e^{-sT_d}G_c(s)}\\&=Y_p(s)+\underbrace{\frac{e^{-sT_d}H_d(s)}{sL_{eq}+e^{-sT_d}G_c(s)}}_{Y_r(s)}\end{aligned} \tag{2}$$

with the superscript d meaning the damped MMC impedance, and subscript r meaning the virtual admittance. As indicated by (2), the voltage feed-forward-based damping scheme can be regarded as employing a parallel virtual admittance $Y_r(s)$ to reshape the MMC admittance, $Y_p(s)$, to improve system stability. In addition, the impedance shape of $Y_r(s)$ is determined by the selection and design of the filtering function incorporated in $H_d(s)$.

3 Proposed Adaptive Damping Method

3.1 Fixed Low-Pass Filtering and Design

As pointed out in [3], MMC can form multiple resonances with the ac system it connects to within the harmonic frequency range, which may cause multiple harmonic oscillations simultaneously. Although multi-tuned narrowband damping control [3] might be a solution, the change in the system resonance condition can significantly shift the frequencies of multiple resonances and make the damping control design more complicated, thereby limiting its application to adaptive damping control. Thus, it is necessary to transform the multiple oscillation issue into a single oscillation issue in order to make the adaptive narrowband damping control more targeted and efficient.

Within the harmonic frequency range, the ac system that the MMC connects to has two important characteristics in terms of its impedance:

- Impedance of a passive grid typically exhibits at most one parallel and one series resonance below $\sim$ 1000 Hz (referred to as the medium-frequency range). It is therefore possible for an MMC to form at most one series resonance with a passive grid within the medium-frequency range.
- There can be two parallel resonances in an impedance of an "active" grid containing power electronics-based converters (e.g., photovoltaic converters or turbine converters), one due to the integrator of the current controller of converter and one due to the shunt filter capacitor; therefore, the MMC can form no more than two unstable resonances with an "active" grid within the medium-frequency range, but with a proper current control design, the amount of unstable resonance can be limited to one.

Based on these characteristics of the ac system impedance within the medium-frequency range, a second-order low-pass filter is adopted in this work to push the termination frequency of the MMC impedance's negative damping into the medium-frequency range, and a

narrow-band damper is then used to address the harmonic oscillation issues within the medium-frequency range. The low-pass filter is given by

$$F_{filter}^{i,v}(s) = \frac{\left(2\pi f_c^{i,v}\right)^2}{s^2 + \sqrt{2}\left(2\pi f_c^{i,v}\right) s + \left(2\pi f_c^{i,v}\right)^2} \tag{3}$$

where f_c is the filter's cutoff frequency, and superscript i, v indicates the low-pass filter in the ac current or the ac voltage control loop, respectively.

Because the low-pass filter reduces the phase margin of the loop gain of controller, the bandwidth of the low-pass filter, $F_{filter}(s)$, must be carefully selected, otherwise the low-pass filter could result in instability of the controller. Assume that the predesigned crossover frequency of the loop gain is f_{cb},and the phase shift generated by F_{filter} at f_{cb} can be calculated by:

$$\theta_f(f)\mid_{f=f_{cb}} = \tan^{-1}\left(\frac{f_c \cdot f_{cb}}{Q \cdot [(f_c)^2 - (f_{cb})^2]}\right) \tag{4}$$

For practical consideration, it is advisable to maintain a worst-case phase margin at approximately 30°. As a result, the minimum cutoff frequency of $F_{filter}(s)$ can be calculated as follows:

$$\tan^{-1}\left(\frac{f_c \cdot f_{cb}}{Q \cdot [(f_c)^2 - (f_{cb})^2]}\right) \geq \phi_m - 30° \tag{5}$$

where f_{cb} and ϕ_m are the predesigned bandwidth and the phase margin of the loop gain, respectively. As an example, if the ac current control is designed to provide a bandwidth of 300 Hz and a phase margin of 60° before applying the filter, the chosen cutoff frequency, f_c, should not be less than 841 Hz.

It should be noted that, in contrast to the existing literature that uses low-pass filters to damp harmonic oscillations, this work does not attempt to eliminate negative damping as much as possible above second harmonic frquency by using low-pass filters with an extremely small cutoff frequency. As a result, it makes the low-pass filters less detrimental to the desired controller dynamics. Also note that the design of low-pass filters presume that the controller is already designed based on the desired dynamics; therefore, if the phase margin is already less than 30°, the low-pass filter should be disabled, or the loop gain should be redesigned to provide a larger phase margin.

3.2 Narrowband Damping Control and Fixed Damper Design

The damping function, $H_d(s)$ in (2), can take different forms depending on the damping requirements. To introduce positive damping at the resonance frequency via damping function, the damper gain should be designed such that the damper behaves like a resistor. However, the damping function itself is also subjected to the time delay effect, which leads to two important considerations:

- The damping gain becomes negative in the frequency range, $[(n + 0.25)/T_d, (n + 0.75)/T_d]$, where $n \in \mathbb{N}$. This can reduce the system phase margin and result in instability within such frequency range. Therefore, the added damping function must be limited in a specified frequency range by combining it with a bandpass filter.
- The added positive damping can also be reduced or turn into negative damping at the target frequency due to delay-induced phase shift. Hence, a delay compensation is required to ensure that the damper emulates a virtual resistor and provides expected amount of damping within the bandwidth of the bandpass filter.

Based on these considerations, the damping function used in this work is designed as:

$$H_d(s) = K_d e^{j\theta} H_{ccf}(s) = K_d e^{j\theta} \frac{2\pi f_b}{s - j2\pi f_r + 2\pi f_b} \tag{6}$$

where $H_{ccf}(s)$ represents a complex-coefficient bandpass filter [10]; f_r represents the center frequency of $H_{ccf}(s)$ in (6)), which is selected as the resonance frequency; f_b signifies the bandwidth of $H_{ccf}(s)$; and K_d is the damper gain. The term $e^{j\theta}$ compensates for the phase lag to which the narrowband damper is subjected at its center frequency, f_r, which makes the narrowband damper act as a resistor at f_r (refer to [3] for more details). Note that $H_{ccf}(s)$ can also be replaced by other types of band-pass filters [11].

3.2.1 Design of K_d: K_d is determined by the level of damping required by the system; however, the improper selection of K_d can cause a shift in the system resonance frequency, f_r. If it moves the resonance frequency outside the damping range defined by f_b, the damped MMC could develop unstable oscillations with the system at the new resonance frequency. Because the existing literature does not provide a proper method for selecting f_b, to avoid the shifted resonance frequency falling outside the damping range, it is recommended that the design of K_d ensures that the real part of the MMC impedance remains the same before and after applying the damper [3, 5]. In other words, the resonance frequency remains unchanged, and the level of damping of the system resonance will be compensated to be positive, effectively suppressing the oscillations associated with the resonance at f_r. This design of K_d is expressed as follows:

$$K_d = x \frac{\left|\mathfrak{Re}\left\{Y_p(j2\pi f_r)\right\}\right|}{e^{j\theta} e^{-sT_d} H_{ccf}(j2\pi f_r)/N_p(j2\pi f_r)} \tag{7}$$

where $x = 2$, $\theta = \angle \frac{e^{-j\omega_r T_d}}{N_p(j\omega_r)}$, $Y_p(j2\pi f_r)$, and $N_p(j2\pi f_r)$ can be referred to as in (1). This design method is hereafter referred to as the "*fixed-gain design*".

3.2.2 Selection of f_b: When the negative damping of the undamped MMC is significant at f_r, especially when the MMC is equipped with a low-pass filter described in

Section 3.1, designing K_d according to (7) might introduce a significant change in the magnitude of the MMC impedance around f_r. If coupled with an improper selection of f_b, this could develop a new magnitude intersection in close proximity to f_r and cause an unstable oscillation.

To better explain this problem, a system with dc voltage-controlled MMC connected to a long overhead transmission line (OTL) is used for illustration, in which the MMC's parameters can be found in Table 1 and Tab. To avoid multiple oscillations simultaneously, a low-pass filter of 1092 Hz is placed in the current measurement. The impedance response of MMC with the filter, denoted as $Z_p^f(s)$, is compared to the impedance of the OTL, $Z_g(s)$, in Fig.2. As can be seen, the "filtered" MMC impedance forms an unstable resonance with the grid at 704 Hz. To damp it, the narrowband damper with K_d designed by substituting $x = 2$ into (7) is employed and the bandwidth, f_b, is varied between 10 Hz, 25 Hz, and 40 Hz. The damped impedance responses are denoted as $Z_p^{fd1}(s)$, $Z_p^{fd2}(s)$ and $Z_p^{fd3}(s)$, and are plotted against $Z_p^f(s)$ and $Z_g(s)$ in Fig. 2. As illustrated, all three designs of narrowband dampers can effectively suppress unstable oscillations at 704 Hz by reducing the phase difference between $Z_p^f(s)$ and $Z_g(s)$ at 704 Hz to below 180°. However, the magnitude responese of $Z_p^{fd1}(s)$ and $Z_p^{fd2}(s)$ again intersect with $Z_g(s)$ at 687 Hz and 682 Hz with phase differences of 189° and 178°, respectively. These new intersections are attributed to the insufficient attenuation rate in the passband of the band-pass filter. Specifically, a damper introduces a certain amount of inductive impedance below f_r and capacitive impedance above f_r. If the compensation for negative damping is significant at f_r, the narrowband damper creates a sharp resonant peak and a resonant dip in the magnitude response of the damped MMC around f_r. This peaking and dipping makes the MMC more likely to interact with the ac system, increasing the risk of forming a new resonance between the damped MMC and the ac system.

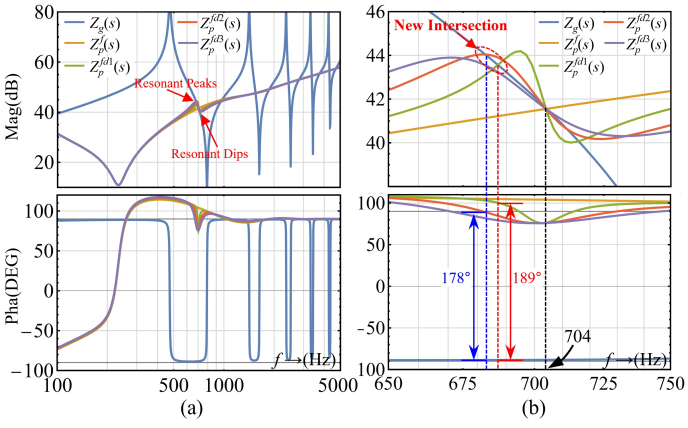

Fig. 2 Effects of narrowband dampers with the fixed damper design on system resonance

According to Fig. 2, the phase difference between $Z_p^{fd1}(s)$ and $Z_g^f(s)$ at 687 Hz is 189°, indicating that a narrowband damper with f_b of 10 Hz simply shifts the unstable resonance condition to another frequency and is not enough to make the MMC stable. A solution to this could involve increasing f_b, which allows the narrowband damper to cover a wider frequency range, including that new resonance frequency. As shown in Fig. 2, the narrowband damper with f_b of 25 Hz shifts the resonance from 704 Hz to 682 Hz, where the phase difference is 178°, which is sufficient to avoid unstable resonance at 682 Hz. On the other hand, the narrowband damper with f_b of 40 Hz avoids introducing a new intersection between $Z_p^{fd3}(s)$ and $Z_g(s)$ around f_r, and therefore it will not excite new oscillations as well.

3.3 Adaptive Narrowband Damper

As indicated in Section 3.2.2, a narrowband damper with a fixed design of K_d and f_b requires an evaluation of its effect on system stability to avoid unintended consequences. In practical applications, it can be difficult to access the grid impedance, making narrowband dampers with a fixed damper design difficult to use; therefore, this subsection proposes a method for dynamically tuning the values of K_d and f_b according to the intensity of the MMC voltage oscillations at f_r, which is hereafter referred to as the "adaptive tuning method." Moreover, the proposed method can also automatically deactivate the narrowband damper when the resonance condition is no longer present by adjusting K_d and f_b to zero.

This method is illustrated in Fig. 3, in which Fig. 3*a* describes the relationship between the adaptive tuning unit and the narrowband damping function, $H_d(s)$; while Fig. 3*b* and Fig. 3*c* depict the block diagrams of the proposed method that adaptively tunes K_d and f_b. The oscillation detection block (see Fig. 3*a*) incorporates an interpolated discrete Fourier transform-based resonance identification algorithm presented in [12], which provides the amplitude of the voltage oscillation at the identified

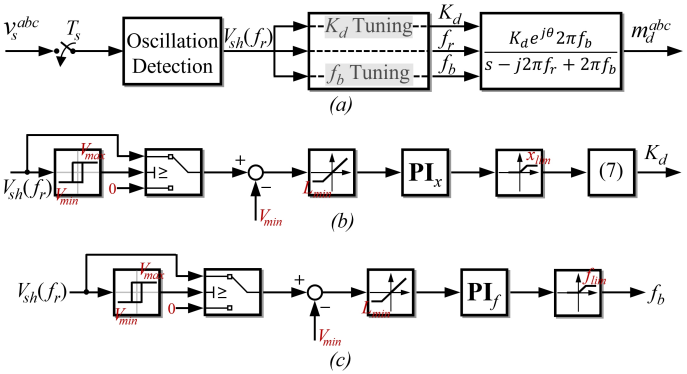

Fig. 3 (a) Overall structure of adaptive narrowband damping control; (b) block diagram of adaptive tuning on K_d; (c) block diagram of adaptive tuning on f_b

resonance frequency, f_r (denoted as $V_{sh}(f_r)$). Note that the voltage measurement, v_s^{abc}, is sampled over a period, T_s, before sending it to the oscillation detection block (see Fig. 3*a*), indicating that the adaptation of K_d and f_b is updated per T_s.

As shown in Fig. 3*a* and Fig. 3*b*, $V_{sh}(f_r)$ is compared to a preset threshold, V_{min}, only when its amplitude exceeds V_{max}. The difference between V_{sh} and V_{min} is then fed into a proportional-integral (PI) compensator, which defines x and f_b. x is then used to calculate K_d based on (7).

Setup of the parameters in adaptive tuning block are now presented:

1) V_{max}*:* In the oscillation detection block, the algorithm used to identify the oscillation frequency requires a comparison between the spectral peak and a preset threshold value. The selection of V_{max} should coincide with the preset threshold value.

2) V_{min}*:* The main objective of the narrowband damper is to mitigate an unstable oscillation at the resonance frequency f_r; however, the magnitude of the frequency component at f_r might not be suppressed to below its steady-state harmonic level, and therefore V_{min} should be chosen at the same level or slightly higher than the background harmonic level defined by the grid code.

3) L_{min}*:* The initial value of L_{min} is set to 0. As a result, the PI compensator ceases to function once V_{sh} is mitigated below V_{min}, which results in the output of the PI compensator maintaining its level. Once the PI compensator's output has been maintained for a certain period, L_{min} is adjusted to negative infinity, which allows the input of the PI compensator to be a negative value. This negative input causes the output of the PI compensator to decrease, which will eventually decrease x and f_b until it reaches 0.

4) x_{lim}*:* The value of x_{lim} can be set to 2 to prevent the PI compensator from excessively amplifying the difference between $V_{sh}(f_r)$ and V_{min}, especially when the difference is substantial due to a rapidly growing oscillation. Otherwise the excessive amplification could cause the narrowband damper to insert a large virtual impedance around f_r, resulting in a significant change in the magnitude of the MMC impedance and leading to undesirable consequences. Note that after the output of the PI compensator saturates at x_{lim}, further adjustments to the narrowband damper would rely solely on the adaptive tuning of f_b.

5) f_{lim}*:* In Fig. 3*b*, if the PI compensator maintain its output at a value smaller than 2, the narrowband damper will move the system resonance downward. As discussed in Section 3.2, a proper selection of f_b should cover the shifted resonance frequency; however, assigning an excessively large value to f_b would contradict the main aim of the narrowband damper, which is to limit the damping effect within a narrow range. Considering that a three-point interpolated discrete Fourier transform [12] is used to estimate the oscillation frequency, a reasonable choice of f_b could be twice the frequency resolution of the discrete Fourier transform.

Table 4 Design of Low-pass Filter and Adaptive Damper

Parameter	Symbol	Value
Cutoff frequency of $F^i_{filter}(s)$	f^i_c	1092 Hz
Cutoff frequency of $F^v_{filter}(s)$	f^v_c	400 Hz
Relay switch-on point	V_{max}	3% $\frac{\sqrt{2}V_N}{\sqrt{3}}$
Relay switch-off point	V_{min}	2% $\frac{\sqrt{2}V_N}{\sqrt{3}}$
Lower limit of saturation dynamic block	L_{min}	$0 \longrightarrow -\infty$
Saturation value of x	x_{lim}	2
Saturation value of f_b	f_{lim}	100 Hz

4 Case studies

To demonstrate the effect of the proposed adaptive narrowband damping control on suppressing harmonic oscillations in MMC-based applications, this section presents two case studies with numerical simulation results obtained with MATLAB/Simulink. The MMC converter and controller designs were previously presented in Table 1 and Table 2; these will be used in each case study. The design of the low-pass filters in the main control loops and of the adaptive narrowband damper are listed in Table 4.

4.1 Harmonic Oscillations Between MMC and Long Overhead Transmission Line

The first case involves a $P\&Q$-controlled MMC connected to a 345-kV long OTL in parallel with a strong grid. Initially, the strong line is open, so the MMC is connected only to the long OTL. To avoid the MMC forming multiple unstable resonances with the long OTL, the simulation is conducted by starting the MMC with the employment of low-pass filter $F^i_{filter}(s)$ in the ac current control loop. For demonstration purposes, initially, only a 50-μs time delay attributed to the zero-order hold circuit of the sampling is included at the beginning of the simulation, and a further 400-μs time delay is added to the MMC at $t = 0.5$ seconds. Upon detection of the oscillation, when both PI compensators sustain their output for 0.4 seconds, the saturation dynamic block's lower limit, L_{min}, is changed from 0 to $-\infty$. To demonstrate that the proposed adaptive damping method can automatically deactivate the narrow damper when the system resonance condition disappears, the ac system to which the MMC connects is switched from the OTL to that of the strong grid at $t = 3$ seconds.

The simulated responses of this system are presented in Fig. 4. At $t = 0.5$ seconds, due to the added 400-μs time delay, the MMC forms an unstable resonance with the long OTL, which drives a growing harmonic oscillation at 709 Hz. The oscillation is measured within three fundamental cycles, and the adaptive tuning unit activates the narrowband damper, as indicated by the increase of K_d and f_b in Fig. 4 *b* and 4*b*. The adaptive tuning unit automatically

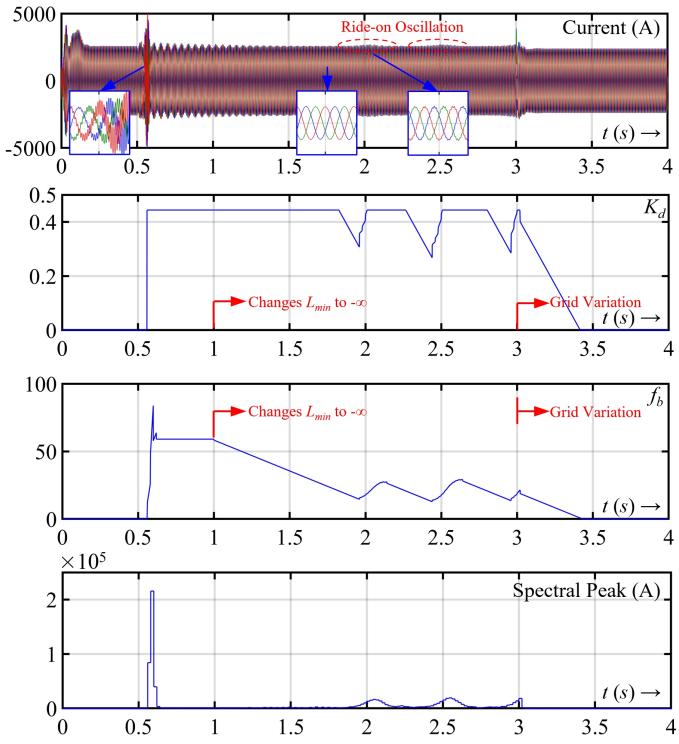

Fig. 4 a) Simulated time-domain responses of MMC current; Output of adaptive tuning unit: b) K_d and c) f_b; d) the spectral peak in fast Fourier transform spectrum from oscillation detection block

regulates and maintains K_d and f_b to the level that is sufficient to bring the amplitude of the frequency component at 709 Hz to be below V_{min}, as shown in Fig. 4 *d*. Note that in Fig. 4*b*, the step change of K_d is due to the output of the PI compensator, which is responsible for adjusting the value of x, and it is limited to between 0 and 2. At t = 0.5 seconds, L_{min} is changed from 0 to $-\infty$; thus, the adaptive tuning tuning can dynamically reduce K_d and f_b. Due to the employment of the narrowband damper, there are no oscillatory components present in the system, and the adaptive damping unit starts to gradually reduce the value of K_d; however, because the resonance condition has not disappeared, once either one K_d or f_b are reduced to a level that makes the narrowband damper insufficient to damp the resonance at 709 Hz, the resonance again starts to drive a growing oscillation at 709 Hz. This dynamic process will repeat until t = 3 seconds, when the resonance condition at 709 Hz disappears due to the ac system switching from the OTL to the strong grid, allowing the adaptive tuning unit to reduce K_d to zero. In other words, the narrowband damper at 709 Hz is deactivated.

4.2 Harmonic Oscillation Between MMC and Offshore Cable Network

The second case is designed to test the effectiveness of the adaptive narrowband damper in mitigating oscillations involving the offshore MMC and the cable network. Due to the bandwidth of the ac voltage control being between 1 and 10 Hz, the low-pass filter in the voltage measurement can be designed with a smaller bandwidth than the filter in the current measurement. In this case, the bandwidth is set to 400 Hz, effectively eliminating the negative damping of the MMC impedance above 460 Hz. This also prevents the MMC from developing multiple oscillations with the cable network within the medium-frequency range during the cable energization. The cable network operates at 66-kV and consists of five 6-mile parallel strings, and it is connected to the offshore MMC through a 66/300-kV step-up transformer. The five strings are connected to the MMC starting at t = 0.1 seconds, with one string being connected every 0.1 seconds.

Fig. 5 shows the simulated responses of the MMC voltage and the adaptive tuning results of K_d and f_b. Because the low-pass filter is applied to the voltage measurement from the beginning of the simulation, the system operates stably without resonance when the first four strings are energized. When the fifth string is connected at t = 0.6 seconds, the MMC forms an unstable resonance with the cable network at 452 Hz, as shown in Fig. 5*b* between 0.5 and 0.6 seconds. The resonance is detected within three fundamental cycles, and the adaptive tuning unit starts to adjust the damper gain and bandwidth, as indicated by the change in K_d and f_b shown in Fig. 5*c* and Fig. 5*d*.

Note that because the PI compensator responsible for adjusting the value of x is not saturated, the added narrowband damper will move the resonance frequency downward; however, the automatic adjustment of f_b ensures that the damping range provided by the narrowband damper covers the shifted resonance. The first time that the adaptive tuning unit sustains the values of K_d and f_b is at $t =\sim$ 1.1 seconds, as indicated by the flat line in Fig. 5*c* and Fig. 5*d*; however, as shown in Fig. 5*b*, the damper designed with this selection of K_d and f_b merely shifts the system resonance condition from 452 Hz to another resonance associated with a slowly growing oscillation. Therefore, at $t =\sim$ 1.55 seconds, the adaptive tuning unit further adjusts the values of K_d and f_b. This process continues until both K_d and f_b are sustained at a level that eliminates the oscillation from the MMC output voltage, as shown in Fig. 5*b* between 2.9 and 3 seconds.

5 Conclusion

This work introduces an adaptive narrowband damping method for suppressing MMC harmonic oscillations. The method involves two parts, low-pass filters in current and voltage measurements, and an adaptive narrowband damper based on ac voltage feed-forward. Unlike

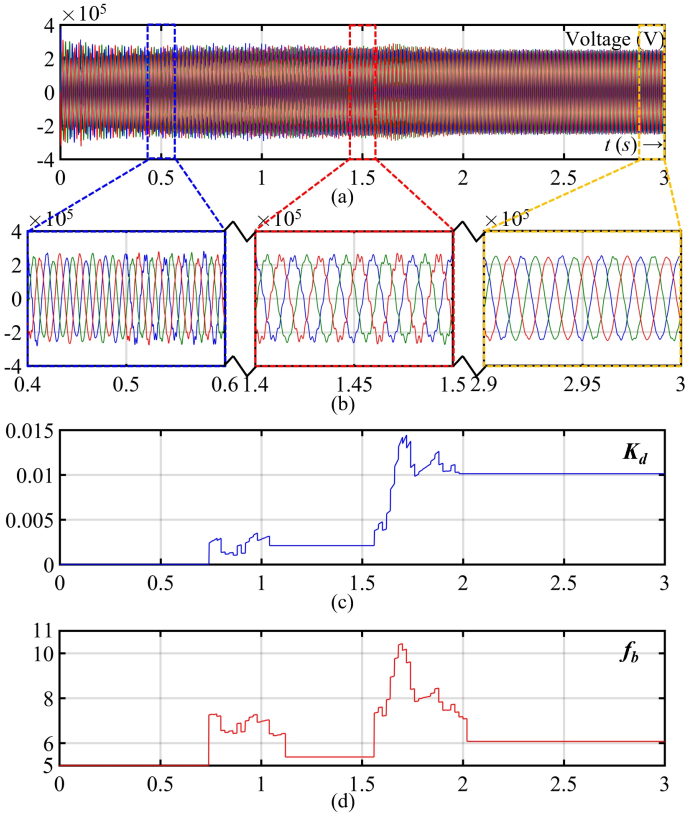

Fig. 5 Simulated time-domain response of MMC: a) overall output voltage; b) zoom-in view of output voltage; c) adaptive tuning results for K_d; d) adaptive tuning results for f_b

the existing literature, low-pass filters are designed to limit the negative damping of the MMC impedance to stay within the medium-frequency range, rather than to remove as much of it as possible from the MMC impedance above the second-order harmonic frequency. The oscillation within the medium-frequency range is then mitigated by the proposed adaptive narrowband damper that can automatically activate, deactivate, and adjust the damper design according to continuous monitoring of the system resonance conditions. Detailed electromagnetic transient simulations validated the effectiveness of the proposed method in improving the harmonic stability of MMC-based systems.

6 Disclaimers and Statements

This work was authored by the National Renewable Energy Laboratory, operated by Alliance for Sustainable Energy, LLC, for the U.S. Department of Energy (DOE) under Contract No. DE-AC36-08GO28308. Funding provided by U.S. Department of Energy Office of Energy Efficiency and Renewable Energy Wind Energy Technologies Office. The views expressed in the article do not necessarily represent the views of the DOE or the U.S. Government. The U.S. Government retains and the publisher, by accepting the article for publication, acknowledges that the U.S. Government retains a nonexclusive, paid-up, irrevocable, worldwide license to publish or reproduce the published form of this work, or allow others to do so, for U.S. Government purposes.

7 References

[1] Saad, H., Fillion, Y.: 'Analysis of harmonics and resonances in HVDC-MMC link connected to AC grid'. Proc. Int. Conf. Power Systems Transients, Seoul, Korea, June 2017, pp. 1–6

[2] H. Lin, T. Xue, J. Lyu and X. Cai, "Impact of Different AC Voltage Control Modes of Wind-farm-side MMC on Stability of MMC-HVDC with Offshore Wind Farms," in Journal of Modern Power Systems and Clean Energy, vol. 11, no. 5, pp. 1687-1699, September 2023.

[3] P. Huang and L. Vanfretti, "Multi-Tuned Narrowband Damping for Suppressing MMC High-Frequency Oscillations," in IEEE Transactions on Power Delivery, vol. 38, no. 6, pp. 3804-3819, Dec. 2023.

[4] P. Huang, H. Wu, L. Vanfretti and O. Gomis-Bellmunt, "Wideband Impedance Passivation of MMCs for Suppressing Harmonic Oscillations," in IEEE Transactions on Power Delivery, doi: 10.1109/TPWRD.2024.3453193.

[5] L. Harnefors, A. G. Yepes, A. Vidal and J. Doval-Gandoy, "Passivity-Based Controller Design of Grid-Connected VSCs for Prevention of Electrical Resonance Instability," in IEEE Transactions on Industrial Electronics, vol. 62, no. 2, pp. 702-710, Feb. 2015.

[6] Wu, H, Wang, X, Kocewiak, ŁH, Hjerrild, J & Kazem, M 2019, Passivity-Based Harmonic Stability Analysis of an Offshore Wind Farm Connected to a MMC-HVDC. in 18th Wind Integration Workshop. 18th Wind Integration Workshop, Dublin, Ireland, 16/10/2019.

[7] P. Huang and L. Vanfretti, "Adaptive Damping Control of MMC to Suppress High-Frequency Resonance," in IEEE Transactions on Industry Applications, vol. 59, no. 6, pp. 7224-7237, Nov.-Dec. 2023.

[8] R. -M. Sallinen and T. Roinila, "Adaptive Bus-Impedance-Damping Control of Multi-Converter System Applying Bidirectional Converters," in IEEE Journal of Emerging and Selected Topics in Power Electronics, vol. 11, no. 1, pp. 567-575, Feb. 2023.

[9] W. Yan, S. Shah, V. Gevorgian and D. W. Gao, "Sequence Impedance Modeling of Grid-Forming Inverters," 2021 IEEE Power & Energy Society General Meeting (PESGM), Washington, DC, USA, 2021, pp. 1-5.

[10] A. Reilly, G. Frazer and B. Boashash, "Analytic signal generation-tips and traps," in IEEE Transactions

on Signal Processing, vol. 42, no. 11, pp. 3241-3245, Nov. 1994.

[11] E. Guest and N. Mijatovic, "Discrete-Time Complex Bandpass Filters for Three-Phase Converter Systems," in IEEE Transactions on Industrial Electronics, vol. 66, no. 6, pp. 4650-4660, June 2019.

[12] D. Agrez, "Weighted multipoint interpolated DFT to improve amplitude estimation of multifrequency signal," in IEEE Transactions on Instrumentation and Measurement, vol. 51, no. 2, pp. 287-292, April 2002.